Sagsnr. 6154-00018B

EROSION

D1.2 Precipitation statistics for selected wind farms

Raingauge

weather radar

present weather sensor

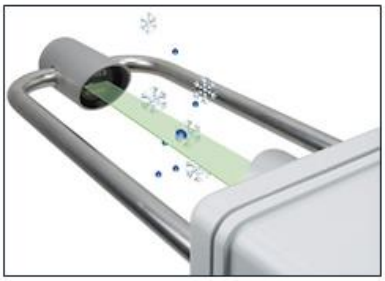

Thies disdrometer

Parsivel² disdrometer

Deliverable: D1.2 (Public)

Authors: Flemming Vejen, Anna-Maria Tilg, Morten Nielsen, Charlotte Hasager

Publication: March, 2018

INNOVATIONSFONDEN / ØSTERGADE 26 A, 4. SAL / 1100 KØBENHAVN K / W: INNOVATIONSFONDEN.DK
www.rain-erosion.dk

D1.2 Precipitation statistics for selected wind farms

Forsidefoto: Instruments for rainfall monitoring.
Udgivet af: Institut for Vindenergi, Frederiksborgvej 399, Bygning 125, 4000 Roskilde
Rekvireres: www.vindenergi.dtu.dk

Preface

This report describes the **Precipitation statistics for selected wind farms** for the EROSION project.

The project is funded by Innovation Fund Denmark and project partners. The project period is from April 1st, 2017 to March 31st, 2020 (3 years).

The aim of the project **EROSION – Wind turbine blade erosion: Reducing the largest uncertainties** is to create knowledge and methods to avoid blade erosion caused by rain and hail. The hypothesis is that by reducing the tip speed of the blades, where rain and hail cause severe blade erosion, a significant extension of blade lifetime can be obtained with reduced maintenance cost and negligible loss of production.

The key objective of EROSION is to enable longer lifetime of wind turbine blades at multi-MW machines. To achieve the objective the project work will include testing of specimen in the rain erosion tester and investigation and analysis of damage on leading edges of blades. Furthermore, the rain in real atmosphere will be investigated from ground-based instruments (disdrometers) and modelling of rain based on rain radar data. Finally a new prototype instrument will be developed in order to measure rain at wind turbines for making decision on control, to set 'erosion safe mode' with regulation of turbines. Much longer lifetime of wind turbine blades and reduced operation and maintenance costs are expected.

Project web-site is http://www.rain-erosion.dk/

Contents

Preface 3
Executive summary 5
1 Introduction 6
1.1 Objectives - why establish precipitation statistics? 6
1.2 Description of selected wind farms 7
1.3 Scheduled experiments 10
2. Precipitation statistics from disdrometer measurements 10
2.1 Introduction 10
2.2 Data 10
2.3 Yearly overviews of disdrometer data (size-velocity histograms) 14
2.4 Comparison of precipitation amount and rain rate measured by the disdrometer and rain gauges 16
2.5 Monthly means of disdrometer data 18
2.6 Influence of wind speed on measured size distribution 22
3. Precipitation statistics from weather stations and radar data 23
3.1 Introduction 23
3.2 DMI weather station data 24
3.3 Precipitation statistics from weather stations 25
3.4 DMI weather radar data 28
3.6 Conversion between radar reflectivity and rain rate 29
3.7 Precipitation statistics based on radar data 31
4. Further work and relation to other WP's 33
4.1 Planned disdrometer campaigns and analyses 33
4.2 Analyses of DMI weather station data near wind farms 33
4.3 Further work on weather radar precipitation statistics 34
4.4 Perspectives for nowcasting of potentially eroding weather conditions 34
References 35

Executive summary

The EROSION project contributes knowledge on the rain events that are hypothesized to be the main cause for the leading edge erosion of wind turbine blades. Observations of rain drop size distribution from the 6-year record from site Voulum in the heart of Jutland is used for detailed analysis. These data are from the HOBE experiment. Observations of rain at the weather stations operated by the Danish Meteorological Institute are the fundament for analysis of long-term rain climate. The novel dual-polarization radars network provides important data with spatial coverage for Denmark and surrounding seas. Finally, a network of disdrometers will be operated within the EROSION project to provide more statistical information on rain events.

The report presents first results from the Voulum site based on disdrometer data. Analysis of disdrometer data shows precipitation types and occurrences during six years. The advantage of this is the information on the drop size distribution. The size of droplets is expected to be of key importance for the leading edge erosion processes, as it is the kinetic energy at the impact that causes erosion initially. Thereafter is presented the analysis of coastal and inland weather stations data. The types of precipitation and their occurrence within one year (2017) are calculated. Finally, results based on dual-polarization radar data for an area over the North Sea are presented.

1 Introduction

1.1 Objectives - why establish precipitation statistics?

In the EROSION project the research hypothesis is that large rain drops cause significant erosion at the leading edges of wind turbine blades. The research hypothesis is sketched in Figure 1.

Figure 1: Sketch of the research hypothesis in the EROSION project.

Perspectives using disdrometers, and measurement of drop size distribution and fall velocity, are further explained in the project report "D1.1 Disdrometers in EROSION" (Hasager and Vejen, 2017).

One of the project goals is to define precipitation erosion classes in Denmark based on observations from disdrometers operated by DMI, DTU, E.ON and Vattelfall during EROSION project. It has been proposed to include weather radar data and precipitation type observations from coastal weather stations operated by DMI in the calculation of offshore precipitation statistics to strengthen the definition of erosion classes in offshore environment. The main objective of this work is to support development of an erosion forecasting model in WP3 by generating statistics and data series, (i) to increase knowledge of key meteorological parameters, (ii) to develop model for calculation of potential risk of eroding conditions at wind farm level. Many studies have shown that droplet size distribution (DSD) and rain intensity is related (e.g. Best, 1950, Kubilay *et al.*, 2013). A basic idea is to utilize rain rates from weather radars instead of DSD parameters in real-time calculation and prediction of droplet kinetic energy and erosion classes.

Key parameters in calculation of droplet kinetic energy and erosion class are drop size disdribution (DSD), liquid volume and terminal fall speed (e.g. Assouline, 2009). Furthermore, hydrometeor type, wind speed and blade tip speed must probably be incorporated to achieve realistic estimates of impact kinetic energy and erosion classes at wind farms.

The content of this report is a presentation of data structures, analyses and statistics on the probability of different rain rates, drop sizes and hydrometeor types. Such statistics is an important step towards establish erosion classes and demonstration of assessment method for precipitation erosion climate at global scale.

1.2 Description of selected wind farms

Selected offshore wind farms in the Danish and Swedish seas are listed in Table 1 and the locations shown in Figure 2.

Table 1: Listing of large offshore wind farms in waters near Denmark

Name	Year	Turbines number	Type	Diameter (m)	Capacity (MW)	Owner
Anholt	2013	111	Siemens SWP3.6	120	400	Ørsted and partners
Horns Rev 1	2002	80	Vestas V80	80	160	Vattenfall, Ørsted
Horns Rev 2	2009	91	Siemens SWP 2.3	93	209	Ørsted
Horns Rev 3	Planned	49	MHI Vestas V164-8.0	164	407	Vattenfall
Kriegers Flak	Planned	72	Siemens Gamesa SG8.0	167	600	Vattenfall
Lillgrund	2008	48	Siemens SWP 2.3	93	110	Vattenfall
Nysted	2003	72	Siemens SWP 2.3	93	166	Ørsted and partners
Rødsand-2	2010	90	Siemens SWP 2.3	93	207	E.ON

The Vindeby offshore wind farm was the first in the world: It was established in 1991 and consisted of 11 0.45 MW Bonus wind turbines. The wind farm has been decommissioned. The Vindeby offshore wind farm in Smålandshavet was standing in a sheltered sea. The first wind farm in harsher environment in the North Sea was Horns Rev 1. Vindeby and Horns Rev 1 are demonstration wind farms. Horns Rev 2, Lillgrund, Nysted and Rødsand-2 consist of Siemens SWP 2.3 turbines while the new planned wind farms will consists of much larger turbines.

The wind climate for the area is shown in Figure 3. The map shows values at 100 m using the extrapolation method as presented in Badger *et al.* 2016. The map is based on Envisat ASAR and Sentinel-1 satellite Synthetic Aperture Radar (SAR) scenes from 2002 to 2012 and from 2014 to present, respectively. Figure 4 shows the average annual precipitation during the period 1961 and 1990 based on observations. From the maps in Figure 3 and Figure 4, it may be noted that variations in wind and rain climate are observed at the different wind farms.

Rain is not measured at the wind farm sites, thus to establish statistics for the areas, we base the analysis on available observations at nearby coastal stations.

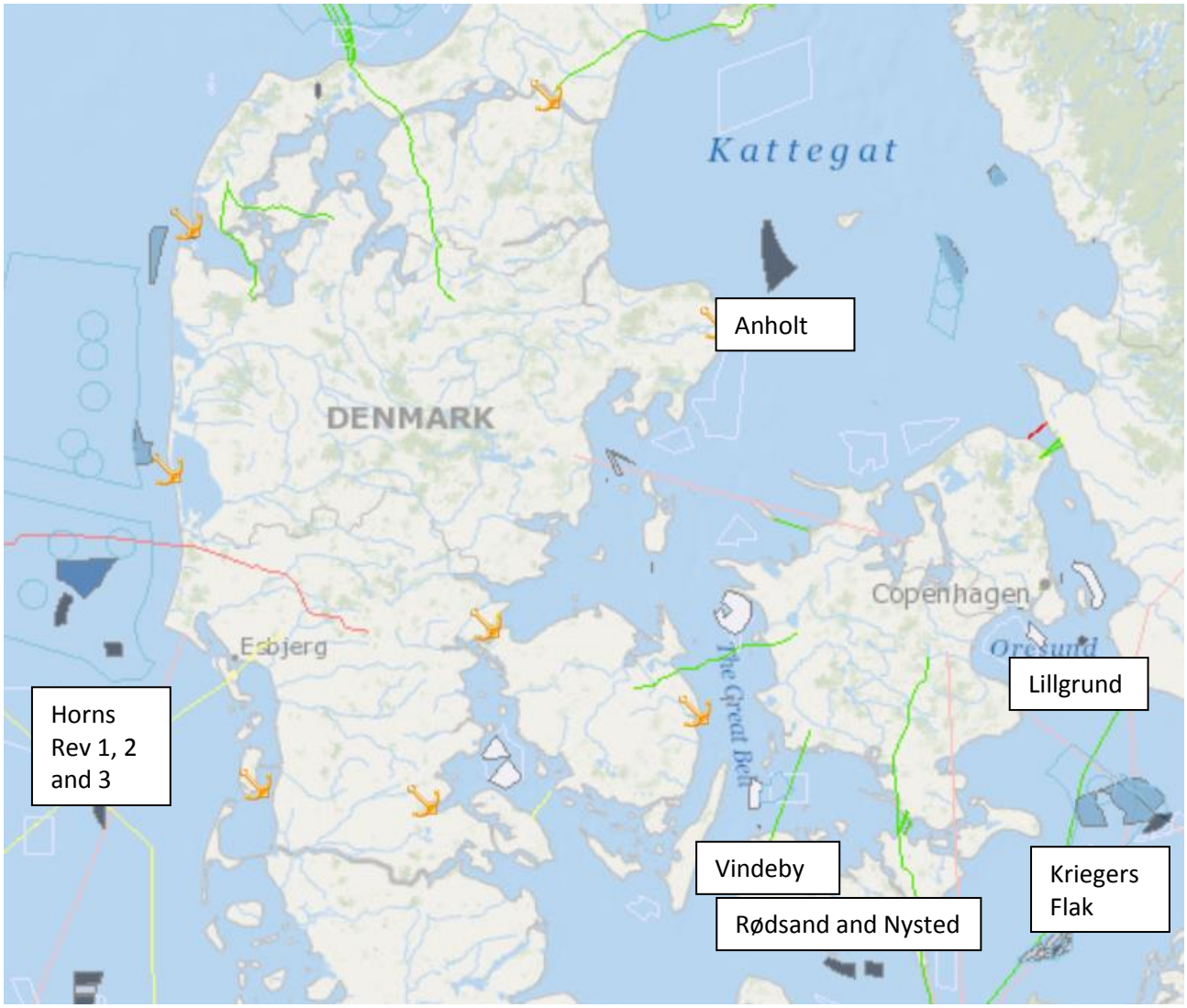

Figure 2: Operational offshore wind farms in grey and consented wind farms in dark blue in the seas around Denmark. Vindeby wind farm is decommissioned. Source: http://www.4coffshore.com/offshorewind/

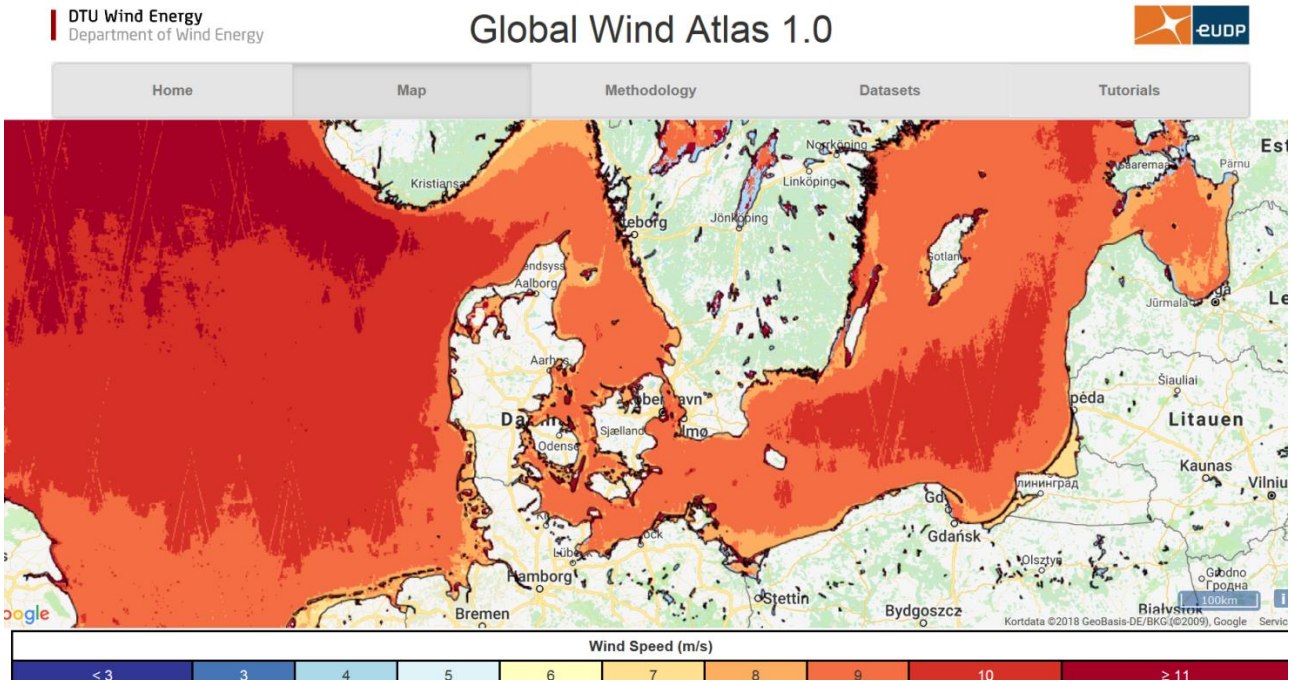

Figure 3: Mean wind speed based on satellite SAR and extrapolated to 100 m using stability information. Source: Global Wind Atlas http://science.globalwindatlas.info/science.html

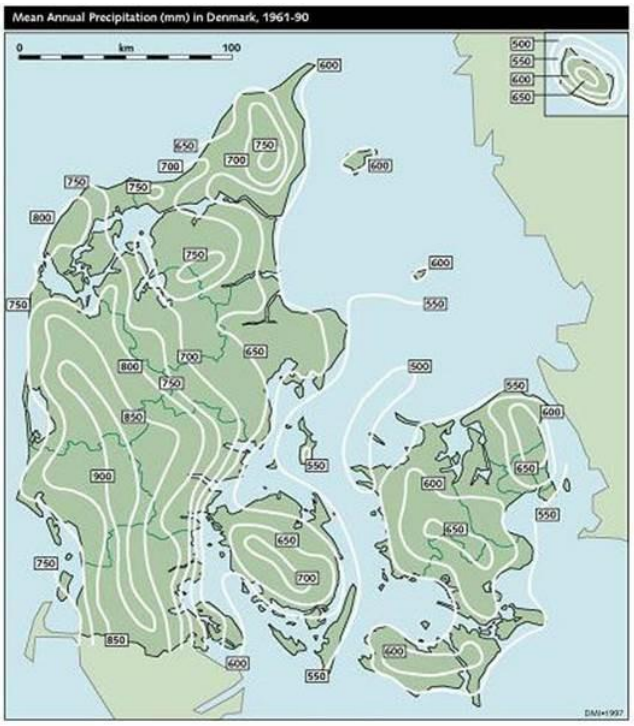

Figure 4: The average yearly precipitation in Denmark in the reference period 1961-1990 measured in mm. Source: DMI Teknisk Rapport 97-8. http://www.klimatilpasning.dk/viden-om/klima/klimaaendringeridanmark/%C3%A6ndringer-i-nedboer/nedboeren-i-danmark-fra-1874-t

1.3 Scheduled experiments

Rain drop sizes, rain rates and hydrometeor types will be investigated using historical data from DMI meteorological station network, DMI dual-polarization weather radars and disdrometers. A number of disdrometers are installed during EROSION WP1 while data from other disdrometers are provided by Aalborg University and the HOBE project[1] in which DMI is participating.

Data series and statistics will be established for analyses of impact time of various hydrometeor types, drop sizes and precipitation intensities. Development of quality assurance methods is an important part of the data processing procedures. As a part of WP1, data series and statistics will be utilized for analyses of the relation between meteorological parameters, kinetic energy and erosion level. Reporting of these activities are beyond the content of this report.

2. Precipitation statistics from disdrometer measurements

2.1 Introduction

To understand and model erosion processes at the leading edge, it is important to know the type, size and velocity of hydrometeors as well as their frequency. An optical disdrometer is a sensor that measures these parameters with a high temporal resolution.

This chapter gives an overview of the relation between the size and velocity of droplets as well their frequency during the year. The yearly amounts and rain rates of disdrometer measurements will be compared with the values of nearby rain gauges.

2.2 Data

Disdrometers are and will be installed at relevant sites (Hasager and Vejen, 2017). Data from three types of disdrometer are available: (i) a 6 year long data series from a Thies disdrometer installed in Voulund test site which is operated by HOBE[2] project; (ii) Parsivel disdrometer data from Aalborg University; (iii) Parsivel[2] data from instruments installed and operated during EROSION.

Thies disdrometer data are analysed in this report to gather experience and knowledge about quality assurance of data, as well as insight into structure and pattern of the relation between drop size distribution, fall velocity of droplets and wind speed.

[1] Center for Hydrology - a Hydrological Observatory and Exploratorium. For further information, see website www.hobe.dk.

[2] Center for Hydrology - a Hydrological Observatory and Exploratorium. The Voulund site is a hydrological test field. The site is serviced and operated in co-operation between Aarhus University, DTU, University of Copenhagen, GEUS and DMI. For further information, see website www.hobe.dk.

A disdrometer measuring campaign of at least one year is expected during EROSION, and various offshore and onshore sites have been selected for installation of instruments (Table 2). There were several aspects to consider for the selection of sites for the disdrometers in the EROSION project. The main location requirements to consider were: 1) access to other meteorological data; 2) differences in precipitation climate; 3) suitable locations for comparison with DMI radar data; and 4) locations as close to wind farms as possible. Table 2 shows a list of the selected sites and Figure 5 shows locations on a map.

Table 2: Selected disdrometer sites

Location	**Operator**	**Specific aspects**
Voulund	DMI	Comprehensive precipitation measurement site.
Thyborøn	DMI	Coastal site
Hvide Sande	DMI	Coastal site
DTU Risø Campus 1	DTU	Concurrent WindScanner lidar
DTU Risø Campus 2	DTU	Concurrent WindScanner lidar plus flexible locations
Horns Rev 3 platform	DTU/Vattenfall	Offshore wind farm

The two DMI weather stations along the west coast of Jutland, Thyborøn and Hvide Sande, are located in a near-offshore environment and may represent offshore conditions. Data from these stations are expected to contribute with valuable information about offshore precipitation conditions. The weather stations measure other meteorological parameters such as wind speed, weather type and precipitation amount which can be used for validation of disdrometer measurements.

Even though the Voulund site is placed in the heart of Jutland far from offshore environment, it offers good opportunities for various disdrometer experiments. Voulund is an experimental field where a variety of meteorological parameters have been measured for more than 10 years in very high temporal resolution.

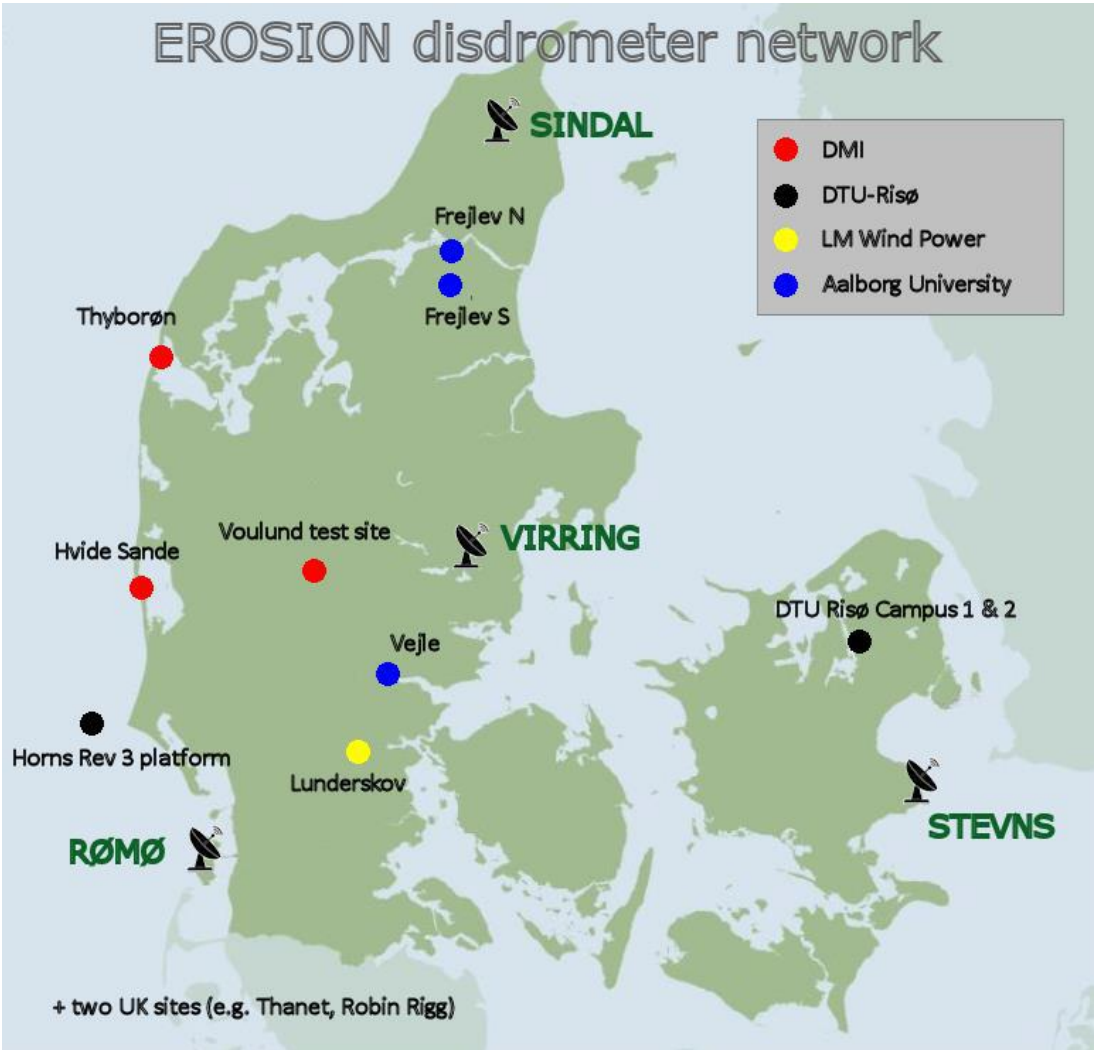

Figure 5: Map of disdrometer locations. It is possible to get access to data from three disdrometer stations owned by Aalborg University. LM Wind Power has planned to install a disdrometer in Lunderskov.

As already mentioned, the installed disdrometer at Voulund test side is a Thies LPM (Laser Precipitation Monitor). It consists of a transmitter and a receiver. The transmitter sends out a horizontal and plane laser light, the receiver consist out of a photo-diode which measured the intensity of the laser light and produces a voltage. When a hydrometeor falls through the laser beam, it is attenuated and the voltage at the receiver changes. Based on the changes of the voltage, an internal algorithm calculates the diameter and velocity of precipitation particles. The Thies disdrometer measures particles with a size between 0.125 mm and > 8 mm (divided into 20 classes) and with a fall velocities between > 0 m/s and > 10 m/s (divided into 22 classes). The steps between the classes are not linear, but the steps are shorter at smaller sizes and velocities than for bigger and faster hydrometeors. The sensor categorizes the measured hydrometeors in one of 440 bins. In sum, data from February 2012 to March 2017 were available for this analysis with a time interval of 1 minute. Table 3 shows the percentage of available data per year.

Table 3: Percentage of available data of disdrometer

Year	Percentage of available values [%]	Notes
2012	82,3	No measurements in January
2013	94,8	
2014	76,4	No measurements in November and December
2015	91.4	
2016	94.6	
2017	18.2	No measurements from April to December

The size and velocity measurements of the disdrometer were raw data. Therefore, some quality control was done which was based partly on the 1min-measurements and partly on estimated events of out the measurements. The start of an event was defined when the number of droplets was unequal to zero. The end of event was defined when the number of measured droplets was again zero. Was the time between the end of an event and the start of a new event shorter than 60 minutes, both events where defined as one event. During the quality control, all numbers of droplets were set to zero which fulfilled one of these criteria:

1. Event had a duration of only 1 minute
2. Event had less than 10 drops in total
3. The rain rate calculated automatically by the disdrometer was zero but the number of droplets not.
4. Particles with a velocity outside of +/- 60% of the calculated terminal velocity of rain / hail / graupel / snow. The terminal velocities are different for rain (Atlas, Srivastava, and Sekhon 1973), hail (Knight *et al.* 1983) and graupel and snow (Locatelli and Hobbs 1974).

The criteria were based on different quality control mentioned in literature (Chen, Wang, and Gong 2016; Friedrich *et al.* 2013; Testik and Pei 2017). However, they refer their quality control only to rain measurements.

In addition to the disdrometer measurements, following meteorological parameters were measured in the same time period with a 10 minutes time interval at Voulund field site.

- Precipitation at rain gauges
- Air temperature
- Relative humidity
- Wind speed and wind direction

One of the rain gauges was in a pit and is called afterwards as rain gauge pit. A fence surrounded the other rain gauge in the winter months to reduce the mismatch of solid precipitation at high wind speeds and is called rain gauge fence.

The yearly total rain amount was around 1000 mm in the analyzed years. The temperature varied mostly between – 10 degrees and + 25 degrees. The wind came mostly from directions between East over South to Northwest with a wind speed up to 5 m/s. Higher wind speeds were related to wind from the Western and Northwestern part.

The interesting parameters for this report were the precipitation measurements and the wind measurements. Table 4 gives an overview of the available data in the different years.

Table 4: Percentage of available data of rain gauge and wind measurements

Year	Rain gauge pit	Rain gauge fence	Wind direction	Wind speed	Notes
2012	100	100	96.3	96.3	
2013	100	100	61.7	61.5	No wind direction and wind speed from end of August to end of the year
2014	43.7	80.7	44.3	44.3	• No rain gauge pit from mid June to end of year • No rain gauge fence in December • No wind direction and wind speed until May and again no measurements in November and December
2015	95.8	95.7	77.2	76.9	
2016	100	100	0	0	
2017	18.7	18.8	0	0	No measurements from April to December

2.3 Yearly overviews of disdrometer data (size-velocity histograms)

The size and velocity measurements of a disdrometer are usually plotted in a so called size-velocity histogram. Figure 6 shows the size-velocity histograms for every year separately including the terminal velocities of the different kinds of hydrometeors. The color of the 440 different bins is based on the logarithmic number of the total sum of hydrometeors in this bin over the year.

The measured pattern was similar for each year. The precipitation was dominated by rain droplets because of the high number of particles along the terminal velocity curve of rain. The higher numbers along the terminal velocity of snow indicates that some snow events occurred as well. The number of measured hail or graupel particles was very low. In comparison, the number of big hydrometeors (> 7.5 mm) and low velocity (< 5 m/s) seems suspicious. It is possible that small insects caused this pattern and were not removed by the quality control criteria. To sum up, the majority of the measured hydrometeors had a diameter between 0.125 mm and 2.5 mm with a velocity between 0.2 m/s and 5 m/s dominated by rain events. The highest number of droplets was found for diameters below 1 mm. However, these plots provided only information about the size and velocity of the measured particles but no information about the amount of precipitation or rain rate. These two parameters will be compared in the next chapter with the measurements of the rain gauges.

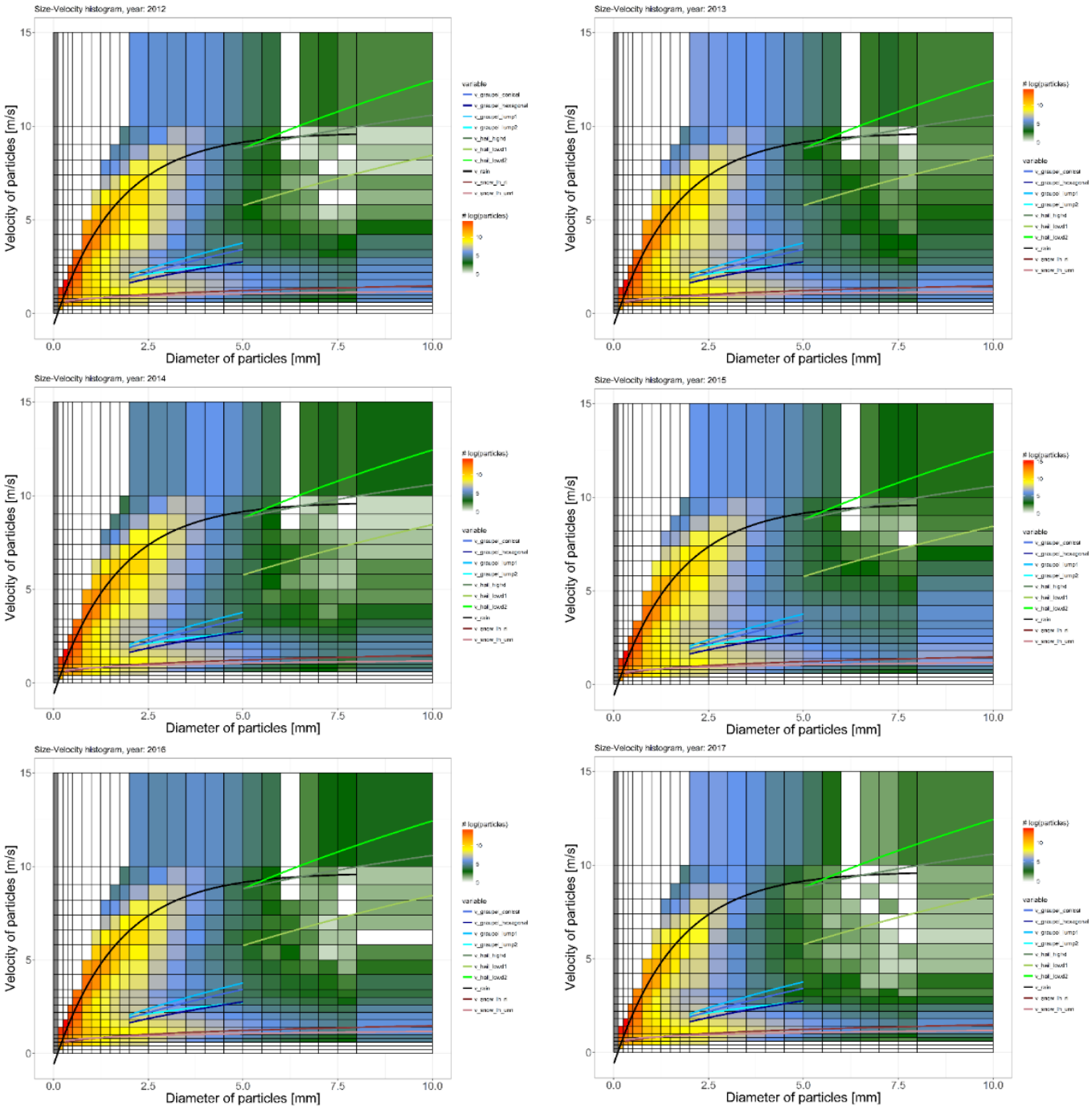

Figure 6: Size-velocity histograms of the years 2012 to 2017. The color represents the logarithmic number of the total number of hydrometeors in the certain bin. The black line is the calculated terminal velocity for rain based on Atlas (1973), the blue and pink colored lines are the terminal velocities of graupel and snow for different conditions based on Locatelli and Hobbs (1974) and the green colored lines are the terminal velocities of hail for different conditions based on Knight (1983).

2.4 Comparison of precipitation amount and rain rate measured by the disdrometer and rain gauges

Usually most locations with precipitation measurements do not have detail measurements of size and velocity. Therefore, only precipitation amount and rain rates can be used to compare the disdrometer measurements with measurements from standard rain gauges. By knowing the diameter of the particles, it is possible to calculate the volume and therefore the amount of precipitation of the disdrometer. This allows the calculation of the rain rate per a chosen time period. As already mentioned, at the field side Voulund measurements of two rain gauges were available for comparison.

Figure 7 shows the comparison of the yearly amount of precipitation of the rain gauges and the disdrometer. Although the time periods of missing values were different for the sensors, the disdrometer measured usually higher precipitation amounts than the rain gauges. Whereas the rain gauges had a total precipitation of around 1000 mm per year and a small variation from year to year, the disdrometer had amounts up to 1500 mm per year and a higher variation from year to year. The higher amount of the disdrometer was influenced by the measured insects characterized as hydrometeors but did not explain all of the difference between the rain gauges and the disdrometer. The rain gauge fence had lower values than the rain gauge pit probably caused by the fact that in the winter month a fence was build up around this rain gauge to reduce the influence of wind on measuring the solid part of the precipitation.

Interestingly, the amount increases were different for the three sensors. For example, the rain gauge pit showed a high increase in January 2013 whereas the others did not show this step like rise. The different purposes of the sensors could be a reason for the different behaviors but all should have registered the events in a comparable scale.

Another option is to compare the rain rates of the sensors. In
Figure 8 the hourly rain rates of the sensors are visualized. For better comparison the limit of the vertical axis was set to 50 mm/h. At the rain gauge pit only one event with slightly over 50 mm/hour was registered whereas for the disdrometer two events with rates above 50 mm/ hour were calculated. Drifting snow could have caused this high rate at the rain gauge pit. All in all, the three subfigures show that the rain rates of the year 2012 to 2017 were different for all sensors. The rain gauge pit had higher rates in the winter and summer months than in spring and autumn. The rates were mostly below 10 mm per hour. At the rain gauge fence the highest values were measured in summer with up to 25 mm/hour. The lower precipitation rates in winter were caused by the fence around the gauge in the winter months and were mostly below 5 mm per hour. Subfigure C shows, that the disdrometer measured especially in the first three month of the year (and once in December 2012) high rates. The reason(s) for these high rates are not easy to identify. Probably wind blowing snow caused these high rates. In the rest of the year, the rates were below 10 mm per hour with a bit higher values in summer. Like for the rain amount the different sensors showed high rain rates for different events. Only for the events in December 2012 the disdrometer and the rain gauge pit showed high rain rates.

All in all, the sensors showed similar tendencies in amount and rain rate but the values itself are only partly comparable. This may be due periods of missing values but also due to different measurement systems and small-scale influences (e.g. fence around gauge in winter). Different authors already analyzed the difference between rain gauges measurements and disdrometer measurements (Lanzinger *et al.*, 2006; Lanza and Vuerich (2009)). They concluded that disdrometers tend to overestimate rainfall rates compared to nearby rain gauges especially at high rainfall rates.

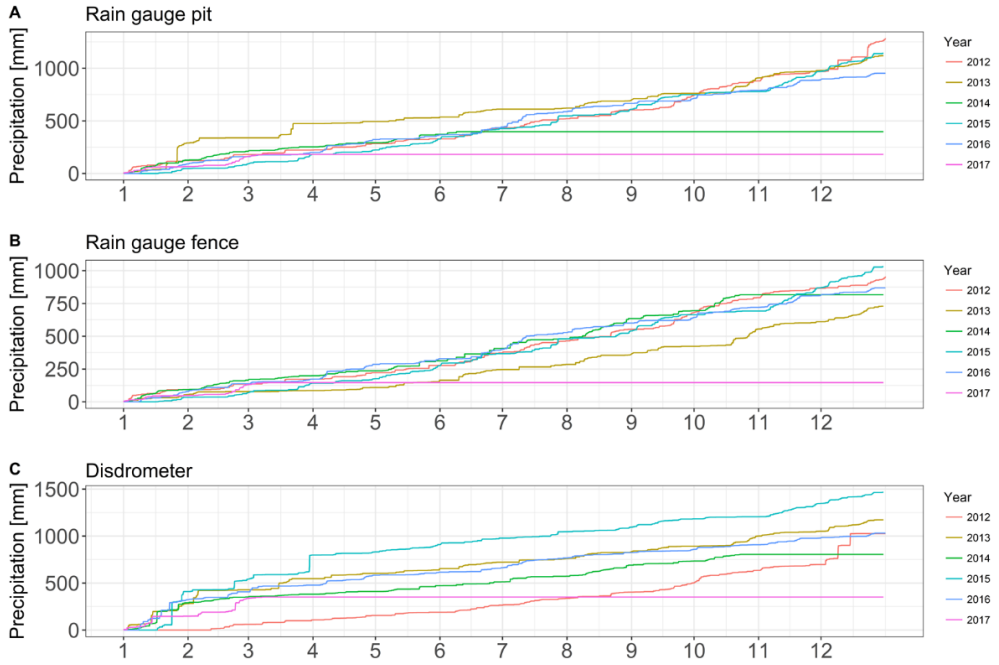

Figure 7: Comparison of the yearly amounts of precipitation at the sensors rain gauge pit, rain gauge fence and disdrometer.

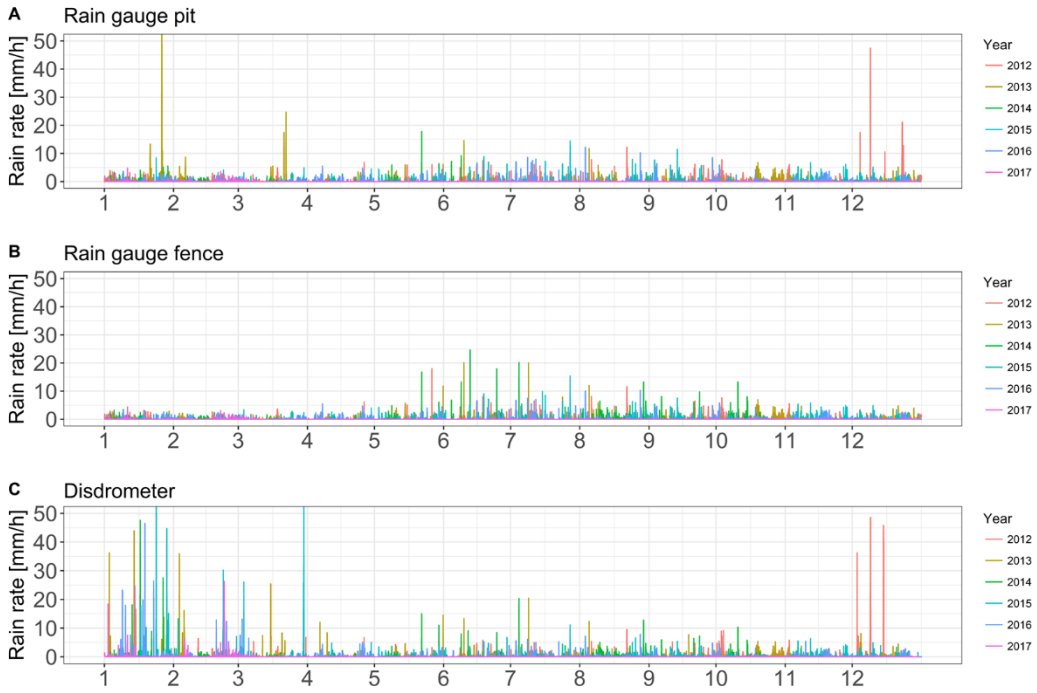

Figure 8: Comparison of the hourly rainfall rates measured by the sensors rain gauge pit, rain gauge fence and disdrometer

2.5 Monthly means of disdrometer data

As we have seen in chapter 2.3, most of the registered drops had a diameter below 2.5 mm. However, Figure 6 provided no information about the monthly variation of the number and distribution of different sizes.

An option to compare these two parameters is the raindrop size distribution or concentration N(D) which is defined as the number of drops per m^3 of air and per mm diameter interval. For Figure 9 the mean concentration for every month was calculated based on the data from the specific month in the years 2012 to 2017. The concentration of small droplets was much higher than the one of big droplets. Up to 0.75 mm the concentration decreased similarly in all moths. For bigger hydrometeors the concentration decrease was lowest in January (black line). In the months February, March and December the decrease was a bit steeper but still lower than for the remaining months. The increase from 7.5 mm to 8 mm in the summer months could be caused by smaller insects and other non-hydrometeors which were characterized wrongly as hydrometeors. To sum up, the events were usually dominated by small droplets up 0.75 mm. Bigger droplets were more frequent in the winter months than in the remaining year. This may be partly due to snowflakes, which can be bigger than rain droplets and partly to higher storm activity in this time period.

For the calculation of the kinetic energy – which is an important parameter in connection to the erosion process – it is important to know more about the fall velocity of the different drops. As already shown in Figure 6, the hydrometeor can take different fall velocities. Turbulence in the air can cause for example these different velocities. Figure 10 and Figure 11 show the mean total number of droplets per m^2 per month based on the data from 2012 to 2017. The mean total number was dived by the number of droplets with a certain fall velocity. As already concluded from Figure 9, the winter months had higher number of droplets as the remaining months. The graphs show that from one single diameter interval more than 100 million of droplets can hit $1m^2$. The bigger the particle, the lower the number. For example, only about 200 000 hydrometeors with a diameter of 5mm hit $1m^2$ in the same time. Droplets with a size up to 0.5mm had fall velocities between 0.2 and 3 m/s. Bigger droplets had higher fall velocities (like already seen in Figure 6). In the winter months the percentage of bigger hydrometeors with lower fall velocity was higher. This is probably caused by the fact that snowflakes are bigger than rain droplets but have lower fall velocity.

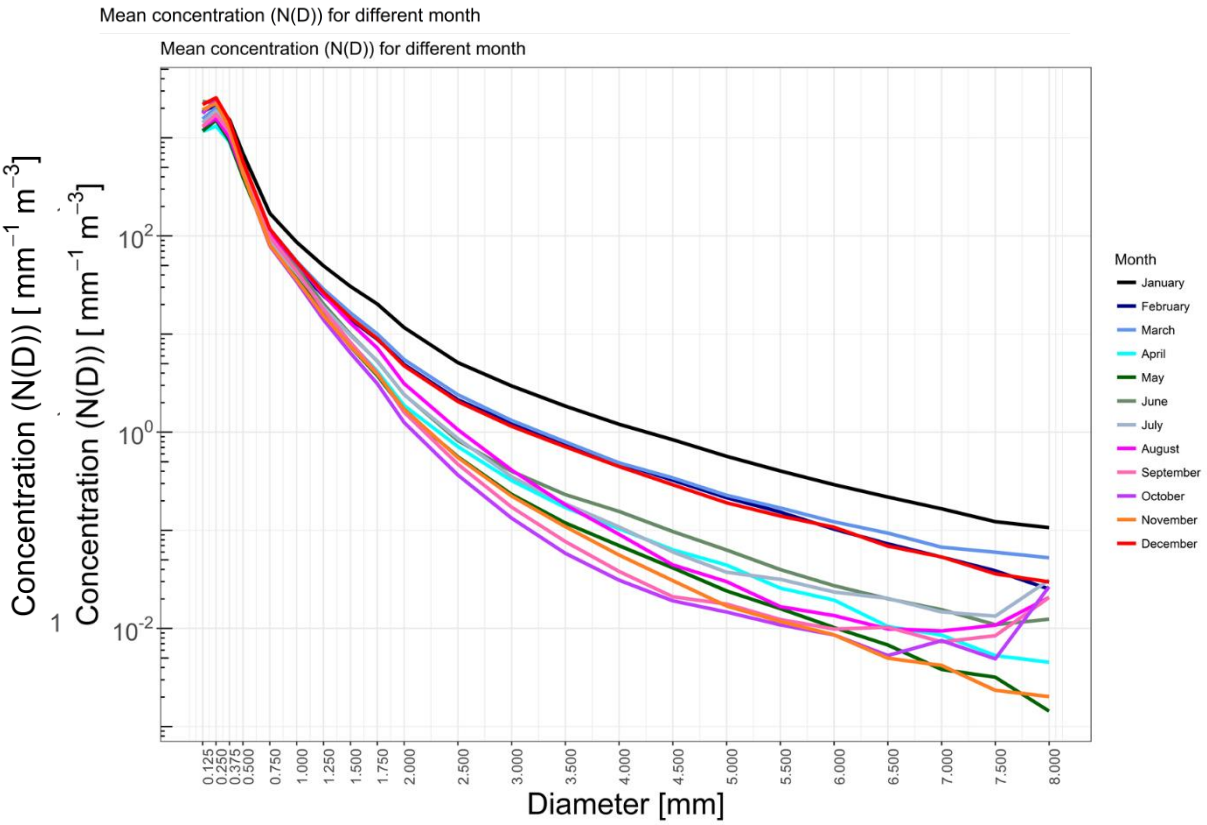

Figure 9: Mean concentration (N(D)) of droplets per m^3 air and per mm diameter interval for different months

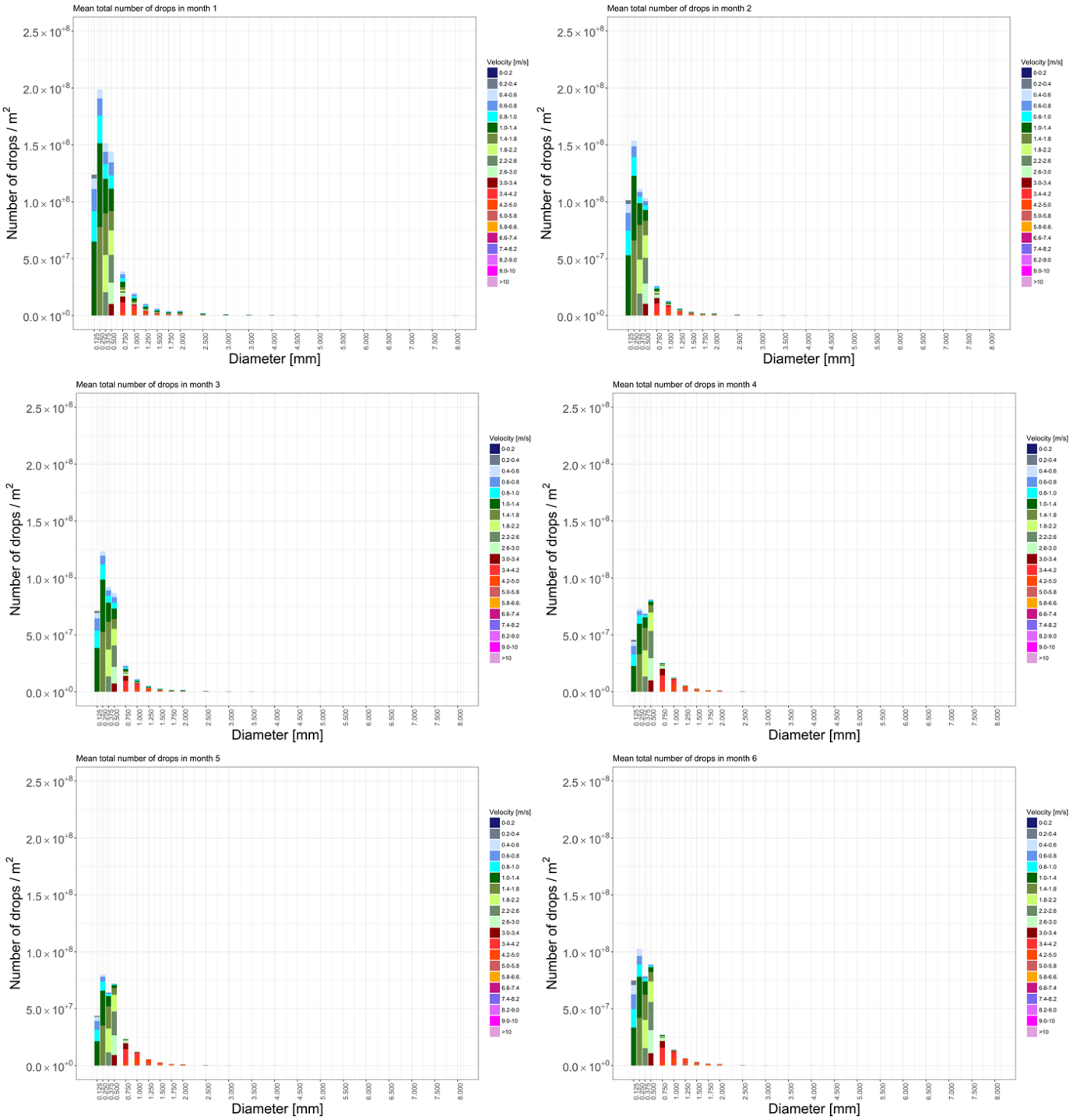

Figure 10: Mean total number of drops per m^2 for different diameters for the months January to June. The mean total number is divided by the percentage of different velocities measured at the specific diameter

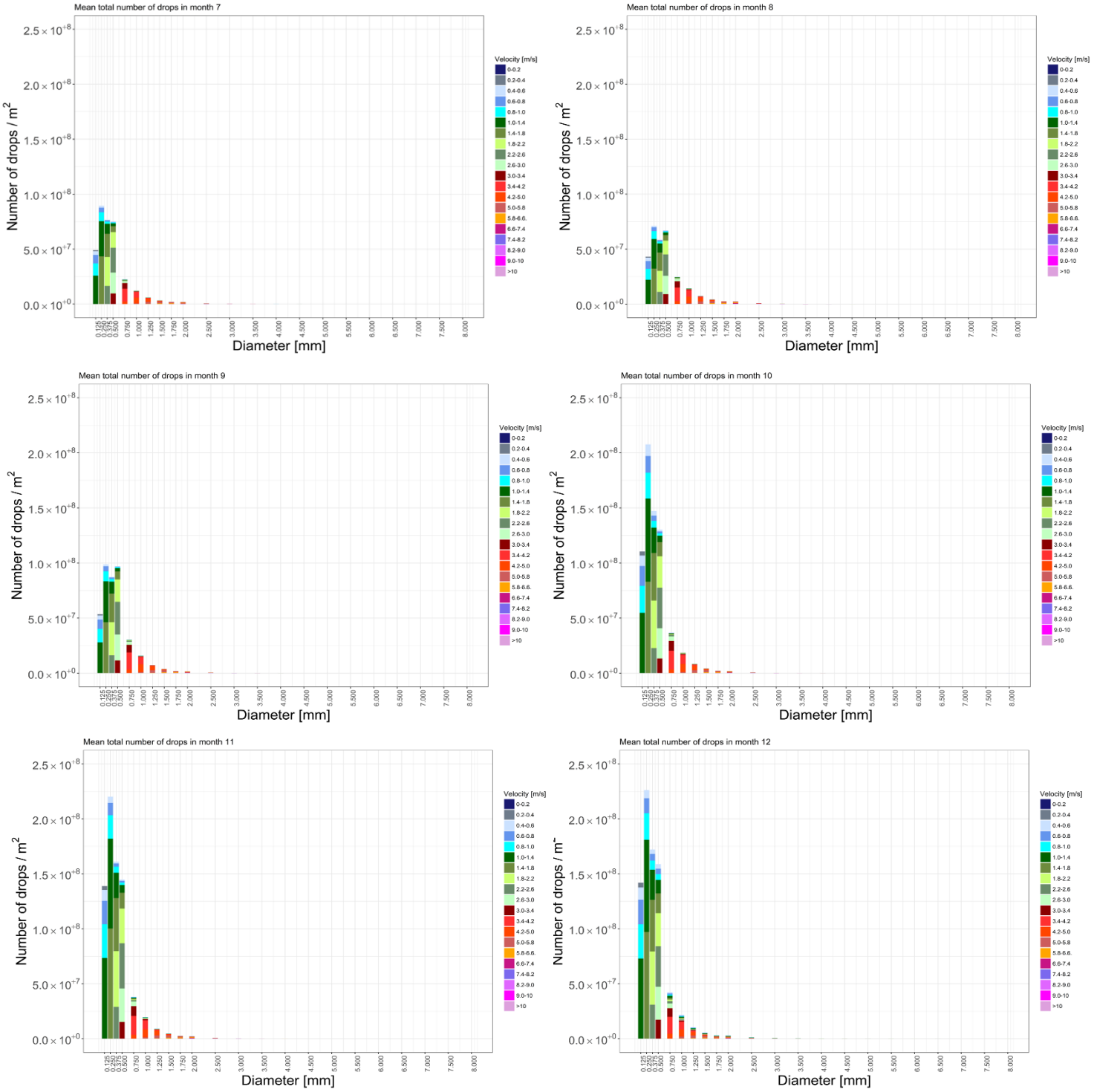

Figure 11: Mean total number of drops per m^2 for different diameters for the months July to December. The mean total number is divided by the percentage of different velocities measured at the specific diameter

2.6 Influence of wind speed on measured size distribution

In the literature it is stated that the wind speed influences the raindrop size distribution of a rain event by increasing the number of small rain drops and decreasing the number of big rain drops at higher wind speeds (Testik and Pei 2017). As this connection between wind speed and number of rain droplets is interesting in this project, the main objective of the following subsection is if such a connection is also visible in the disdrometer dataset of Voulund.

This analysis is based on the estimated rain events from the year 2013. So no snow, graupel or hail events are included. For all rain events the mean wind speed was calculated as well as the sum of droplets smaller or equal to 1 mm. Events with a duration longer than 2500 minutes (> 1 day) were neglected, as these events were extremely rare and therefore did not represent a normal event. The remaining events where categorized based on their duration, as the type of precipitation (stratiform or convective) is not available for this analysis. With the categorization by the duration, it was assumed that the driving mechanisms of the events are the same. Shorter events are more likely convective events. Longer events are more likely stratiform events. In this analysis, the connection between the number of small droplets (NSD) and the wind speed for events with a duration between 11 and 120 minutes was analysed. These chosen durations should mainly include convective driven rain events and exclude extreme short time events with a duration of 10 minutes and stratiform driven rain events with frequently longer durations. In addition, rare events with more than 30000 small droplets were neglected. In total 243 events fulfilled these requirements.

The dependence of the NSD on the wind speed was investigated with a simple linear regression. For this linear regression all above chosen events where considered to find a connection between the NSD droplets and the mean wind speed of an event. As the residuals of the untransformed data did not show a normal distribution, the parameter NSD was transformed with a cube root.

The results of the linear regression showed a slight decrease of the NSD with increasing wind speed but with a non-significant slope. As Figure 12 shows, the number of events at high mean wind speeds are rare and could influence the result of the linear regression. Therefore, in an additional step all events with a mean wind speed above or equal to 8 m/s were neglected. Also for this case the slope is slightly negative but not significant – indicated by the p-value above 5%. Figure 12 shows the regression lines of both versions on the original scale. They show both a nearly horizontal line, which was already indicated by the slightly negative but non-significant, calculated slopes.

All in all, it can be concluded, that for the chosen events no linear connection between number of small droplets and mean wind speed was given.

The connection found by (Testik and Pei 2017) was only partly seen in the data of Voulund as in some events at Voulund in 2013 the number of small droplets increases with increasing wind speed but not in general. It seems that the selection of events plays an important role. Further steps in analyzing possible connections between wind speed and number of droplets are needed – for example the analysis of the parameters of a droplet size distribution / concentration (N(D)) comparing different events.

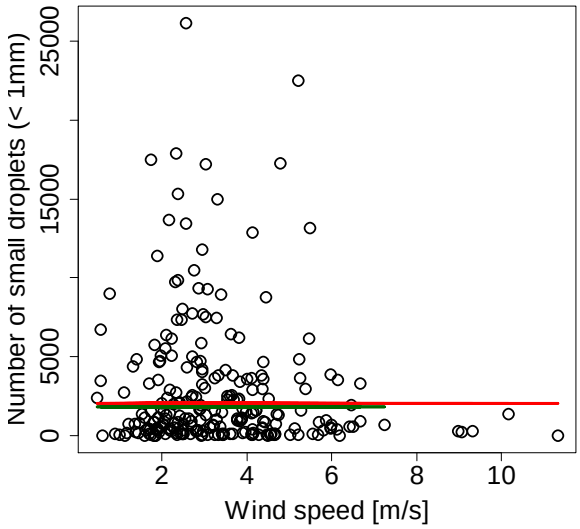

Figure 12: Regression plot on original scale with two regression lines. The red regression lines includes the events at high wind speed, the green one does not include them

3. Precipitation statistics from weather stations and radar data

3.1 Introduction

A key objective in the project is to develop nowcasting methodology to predict the risk of blade erosion. The engine for forecasts will be real-time analyses of data from weather radars and numerical forecasting models operated by DMI. Therefore, the information content of radar rain parameters will be investigated.

A disdrometer provides detailed information on particle size distribution (DSD) for a range of precipitation types. Moreover, other standard parameters of the instrument are such like hydrometeor type, precipitation intensity and kinetic energy which are calculated for the total amount of particles detected for a certain period of time.

Disdrometers installed during EROSION are planned to collect at least one year of data during measurement campaigns. This period length may be a limitation factor for the estimation of representative statistics on offshore precipitation environment, but data will be very useful to establish a methodology for conversion between radar measurements and parameters relevant for prediction of potentially eroding weather conditions.

While weather stations and disdrometers are point measures normally installed onshore, weather radars scan the atmosphere up to large ranges. Therefore, perspectives are related to the inclusion of weather radar data, not only for offshore weather monitoring but also for calculation of offshore statistics.

Meteorological parameters from DMI weather stations and data from weather radars are stored in historical archives. Based on these data it will be possible to make calculations of relevant statistics, such as impact time of different hydrometeors and rain intensities, for very long time series, i.e. periods of up to 16 years. Data from measurement campaigns and long time series are expected to strengthen the possibilities for developing a methodology for prediction of potentially eroding conditions.

3.2 DMI weather station data

DMI operates a number of weather stations that measure a variety of meteorological parameters relevant for statistics, such as weather type, air temperature, wind speed and amount of precipitation. Figure 13 shows stations equipped with a present weather sensor (PWS) of type Vaisala FD12P.

The technique behind PWS measurements is based on the principle that light[3] scattered from a hydrometeor is proportional to the volume of the particle. This relationship is quite stable for liquid droplets because of the more or less spherical shape, but even though it becomes more unstable for snow the scattering is proportional to the average volume of snow. Analyses of temporal variations of scattering, outliers, precipitation intensity and air temperature are used as additional parameters in the weather type classification algorithm. Because hail is normally mixed with heavy rain, the hail detection may be a little uncertain (Vaisala, 2002). The use of fixed temperature thresholds in the weather type detection scheme may be a source of uncertainty. Unreliable classification may also occur for very low intensity or sparse detection of hydrometeors.

A number of weather stations are well suited for estimation of near-offshore statistics due to their location relatively close to relevant offshore wind farms in Danish sea areas. All stations measure meteorological parameters in very high temporal resolution (10-minute). Most of them were upgraded to this measuring frequency during the years 2001-2002.

[3] The instrument measures in the near infrared part of the electromagnetic spectrum.

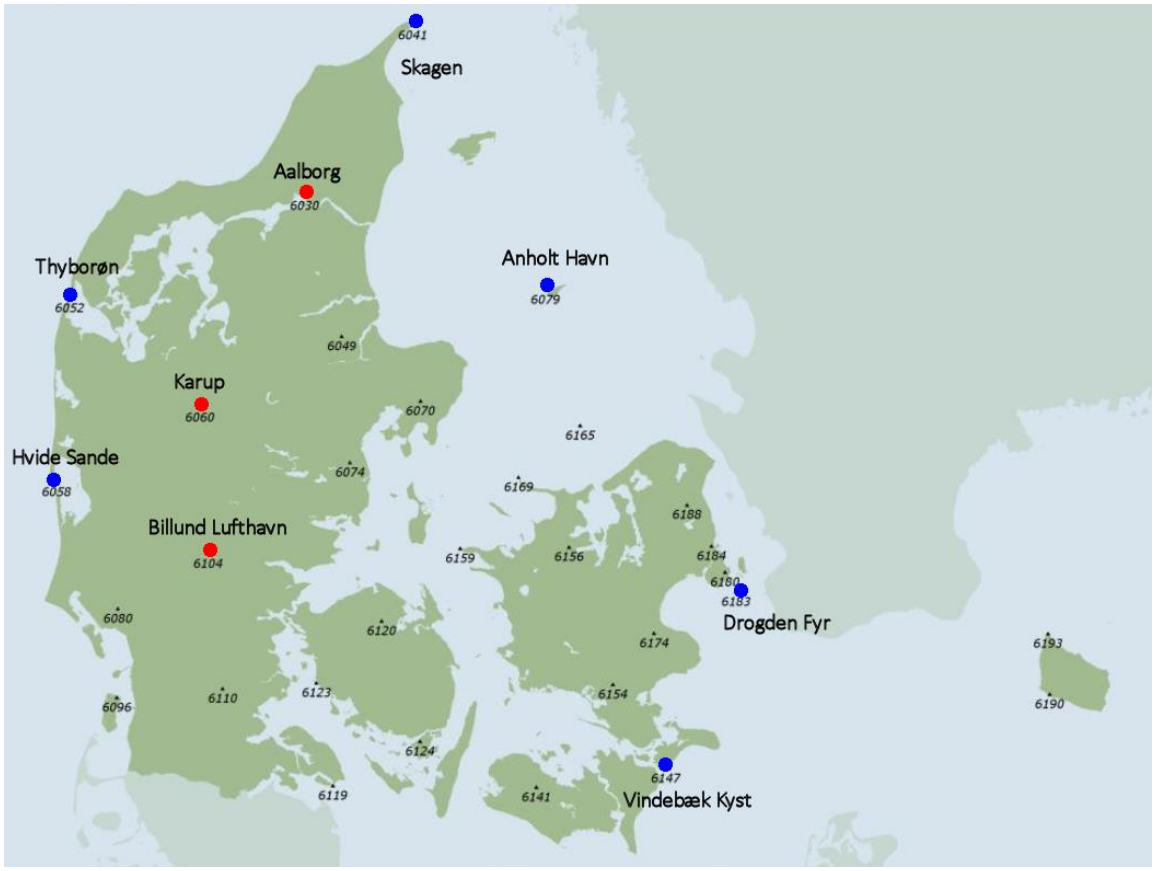

Figure 13: DMI network of weather stations observing weather type - many of them also measure wind speed, air temperature and precipitation amount. Blue dots = stations that may be relevant for estimation of statistics near existing or planned wind farms. Red dots = inland stations used for estimation of statistics to compare with coastal stations

3.3 Precipitation statistics from weather stations

The long time series of high resolution meteorological observations from near offshore weather stations offer the opportunity to establish precipitation statistics on a more solid basis than one year measurement campaigns.

One interesting aspect to further examine is the long term frequency of erosion critical precipitation at locations near relevant wind farms selected for this specific study. In Table 5 is shown weather stations relatively close to existing or planned wind farms. These near-offshore stations are probably representative for the offshore precipitation environment at the wind farms.

Table 5: Sites selected to establish precipitation statistics near offshore wind farms

Weather station	Environment	Specific aspects
Hvide Sande	Near-offshore	Relatively close to Horns Rev wind farms
Thyborøn	Near-offshore	Data useful for Horns Rev analyses
Anholt Havn	Near-offshore	Anholt wind farm
Vindebæk Kyst	Near-offshore	Nysted and Rødsand wind farms
Drogden Fyr	Near-offshore	Lillgrund wind farm and Kriegers Flak planned wind farm

Examples of precipitation statistics are shown in Table 6 and Table 7.

To get an impression of the offshore environment, e.g. near Horns Rev, three stations along the west coast of Jutland (Skagen, Thyborøn and Hvide Sande) have been chosen for the statistical calculations, assuming they represent the precipitation climate over the North Sea. Table 6 shows the frequency of various precipitation types during all seasons in year 2017 given as number and percentage of 10-minute observations at inland and near-offshore weather stations (Figure 13).

The probably most potentially harmful precipitation types such as heavy/violent rain and solid precipitation was relatively rare in the period, but even though the frequency and duration time was at a minimum it may still be significant for blade erosion. Heavy and violent rain was observed in 0,9-1,4 % of all precipitation observations corresponding to approximately 25-40 hours of duration, while freezing rain, ice pellets and snow grains were detected in 0,4-1,0 % of all precipitation observations, or 13-27 hours of duration. It will be interesting to see similar statistics for a much longer period of time for the stations in Table 5.

Table 6 shows the frequency of various rain types and their average and maximum 10-minute rain rates during the heavy rain season May-September 2017. Large short time variations of rain rate may be observed within 10 minutes, especially in heavy and violent rain showers. The highest rain rates observed during the period were 26,4 in heavy rain and 36,0 mm/h in heavy showers. For automatic detection of precipitation type the PWS instrument uses analyses of rain rate variations during the observation period. Rain rate variations exceeding a certain threshold cause the precipitation to be classified as showers, and the 10-minute rain rate average is less representative for the observation period.

The main advantage of weather stations is the long time series. Few drawbacks of this data type could be: (i) stations are not real offshore; (ii) precipitation intensity in finer time scale is not available. This underlines the potential of incorporating weather radar data in the analysis of offshore precipitation, as they provide detailed snapshots of precipitation intensity for very large areas.

Table 6: Number of 10-minute observations and percentage frequency in 2017 for various hydrometeor types detected at a number of near-offshore and inland DMI weather stations. Inland stations: Aalborg, Karup and Billund Lufthavn. Near-offshore stations: Skagen, Thyborøn and Hvide Sande (see Table 5)

Hydrometeor type	Relative intensity	Near-offshore		Inland	
		N	%	N	%
Drizzle	slight	3197	19,03	1162	6,39
	moderate	3327	19,80	374	2,06
	Heavy	82	0,49	38	0,21
Rain	slight	7987	47,53	11433	62,83
	moderate	1325	7,89	1715	9,42
	heavy	147	0,87	226	1,24
	violent	0	0,00	8	0,04
Melting snow	slight	83	0,49	248	1,36
	moderate	5	0,03	7	0,04
Snow	slight	575	3,42	1889	10,38
	moderate	0	0,00	935	5,14
Freezing rain	all	35	0,21	135	0,74
Ice pellets	all	24	0,14	26	0,14
Snow grains	all	14	0,08	0	0,00
Hail	all	3	0,02	1	0,01

Table 7: Statistics based on 10-minute observations of hydrometeor type and rain rate for precipitation classified as drizzle, rain and rain showers at 3 near-offshore DMI weather stations (see Table 5) based on data collected during the period May-September 2017

Precipitation type	Intensity category	N	Pct	Average rain rate [mm/h]	Maximum rain rate [mm/h]
Drizzle	slight	392	6,84	0,06	1,8
	moderate	459	8,01	0,32	2,4
	heavy	25	0,44	1,01	3,0
Rain	slight	1260	21,98	0,75	9,0
	moderate	271	4,73	3,52	12,0
	heavy	50	0,87	10,73	26,4
Rain showers	slight	3007	52,45	0,32	21,6
	moderate	207	3,61	3,37	13,2
	heavy	62	1,08	10,80	36,0

3.4 DMI weather radar data

DMI operates a radar network of five dual-polarization (dual-pol) C-band Doppler weather radars (Figure 14), hereafter called dual-pol. A dual-pol weather radar is a remote sensing instrument that measures reflectivity of objects in two polarizations, horizontal and vertical, in a given volume in the atmosphere. The radar scans in azimuth at a number of elevations and detects the atmospheric content of hydrometeors and their properties.

Various sophisticated parameters (or moments) are measured by dual-pol radar technology, such as: (i) differential reflectivity (uses the difference between vertical and horizontal reflectivity) which is a good indicator of mean size and shape of droplets in a volume; (ii) correlation coefficient which is a measure of how similarly the two polarizations are behaving in a pulse volume and that is especially useful for discrimination between meteorological and non-meteorological targets. Dual-pol moments can be used in hydrometeor classification algorithms (e.g. Straka, Zrnic and Ryzhkov, 2000), and the classification method used at DMI is described in Gill, Sørensen and Bøvith (2012). The radar network provides radar data in high temporal and spatial resolution, i.e. 500×500 m^2 pixel size and 10-minute scans up to 240 km range.

Rain rates calculated from radar reflectivity data and classification of hydrometeor type is expected to be very useful for the development of an algorithm for estimation of kinetic energy and erosion class in fine spatial and temporal scale.

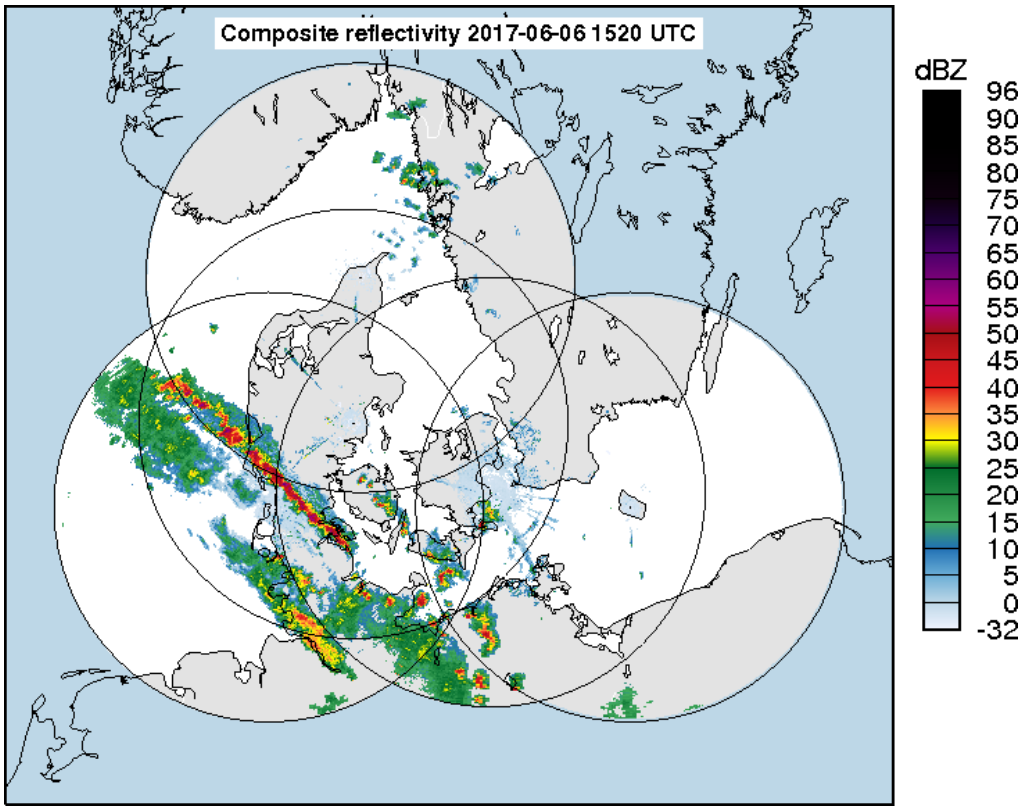

Figure 14: DMI's weather radar network shown with an example from 6 June 2017 at 1520 utc. The unit dBZ indicates the relative rain rate

3.6 Conversion between radar reflectivity and rain rate

Radar measurements of backscattering by hydrometeors are directly related to radar reflectivity Z. Both the reflectivity and the rain rate R is related to integrations of DSD; R through the sum of droplets per time unit, and Z through the total backscattering from droplets in a volume. It is found, that $Z=\sum nD^6$, where n=number of droplets and D=droplet diameter (Battan, 1973). Extensive research on the data structure of Z and R has employed a general empirical expression of the form $Z=AR^b$, where A and b are constants (Battan, 1973). A widely used expression for stratiform rain, $Z=200R^{1.6}$, was developed by Marshall and Palmer (1948). Z-R relationships have been developed for a large range of precipitation types (e.g. Šálek *et al.*, 2004).

Due to the Earth curvature and the propagation of the radar beam, radar quantitative precipitation estimate (QPE) may not represent surface rainfall properly because the radar beam is far above the ground at longer ranges. During non-standard atmospheric conditions, such as temperature and humidity inversions, propagation of radar beam is downward bended. This may result in severe false echoes from ground targets. Furthermore, targets near the radar station may cause persistent false echoes. Range-dependent errors are mainly due to the vertical variation in the reflectivity profile with distance, and at longer distances the radar may overshoot shallow precipitation areas. A comprehensive summary of errors in radar detection of hydrometeors can be found in Šálek *et al.* (2004). Fortunately, severe false echoes do not normally occur during precipitation.

Systematic bias in estimation of radar rain rates is introduced by using uniform Z-R relationship to represent varying Z-R relationships. Range dependent errors are related to the decreasing correlation between what the radar measures aloft and the surface rain. Also radar beam occultation may play a role in reliable rain rate estimation. Random errors come from the radar signal noise referred to above such as false echo effects. Many techniques for estimation of reliable radar rain products have been proposed (Brandes, 1975, Krajewski, 1987, Smith and Krajewski, 1991, Rosenfeld *et al.*, 1994, Gabella and Amitai, 2000, Sinclair and Pegram, 2005, Chumchean *et al.*, 2006, Haberlandt, 2007).

The QPE estimation technique (quantitative precipitation estimate) implemented at DMI is based on the so-called BALTEX approach (Michelson *et al.*, 2000), and the implementation is described in more details in He *et al.* (2011). Firstly, a uniform Z-R relation is applied to estimate radar QPE fields, and secondly, the resulting systematic biases as well as a range dependent noise are adjusted using calculated correction factors for each pixel in the radar composite image. These factors are based on analyses of the spatial structure of biases between unadjusted radar QPE and data from the raingauge network. An example of a QPE field is shown in Figure 15.

The analyses presented in this report have been made for rainfall over a period of 6 hours. It is assumed, that the correction factors estimated can be applied to the individual radar images with reasonable results. The example in Figure 16 shows a comparison between a raingauge and a radar time series calculated by adjustment of each radar image. In the example, the time resolution of radar data has been artificially increased to 1-minute by interpolation between each individual radar frame.

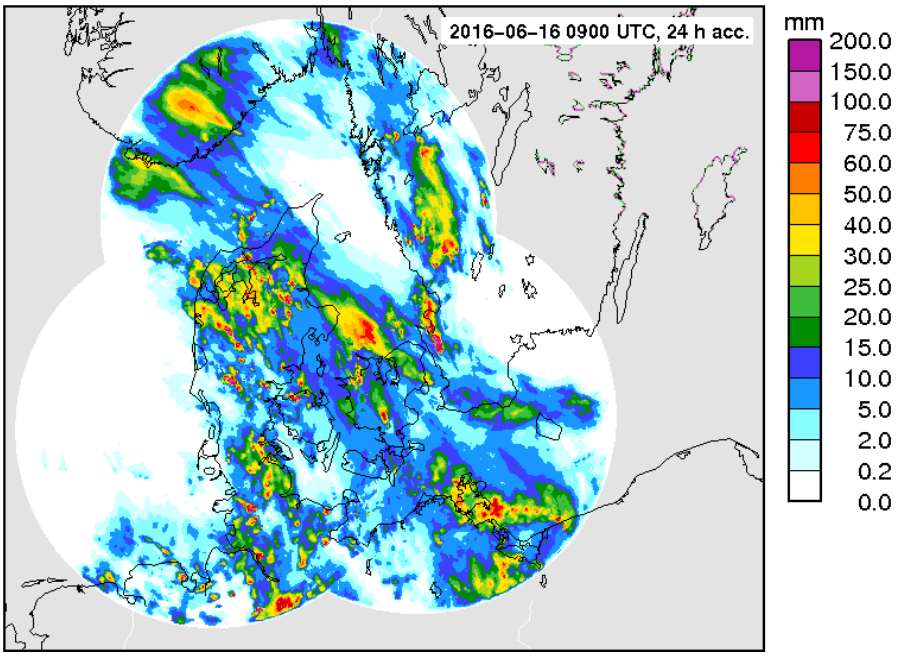

Figure 15: Radar QPE (quantitative precipitation estimate) field on 16 June 2016 at 0900 utc

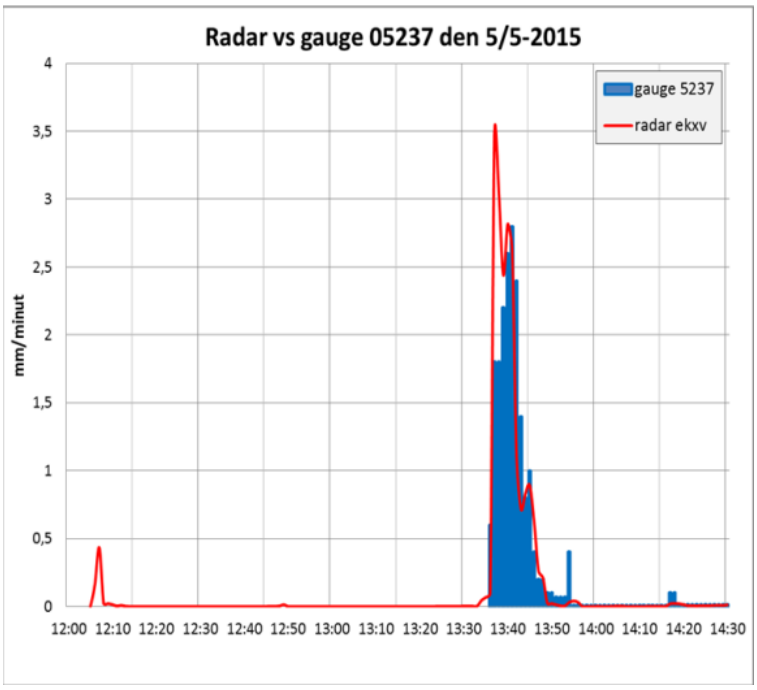

Figure 16: The example shows a comparison between a raingauge (Vejle Pumpestation) and a radar time series calculated by adjusting each radar image (Virring radar data)

3.7 Precipitation statistics based on radar data

Based on radar data, rain rate statistics has been calculated for a sector along the west coast of Jutland (Figure 17) for June-August 2017, which are the months statistically most affected by heavy or violent rain and hail. The purpose of this first approach was primarily to develop methods and software for calculation of comprehensive statistics. Next step will be to extend data analyses to a much longer period of time.

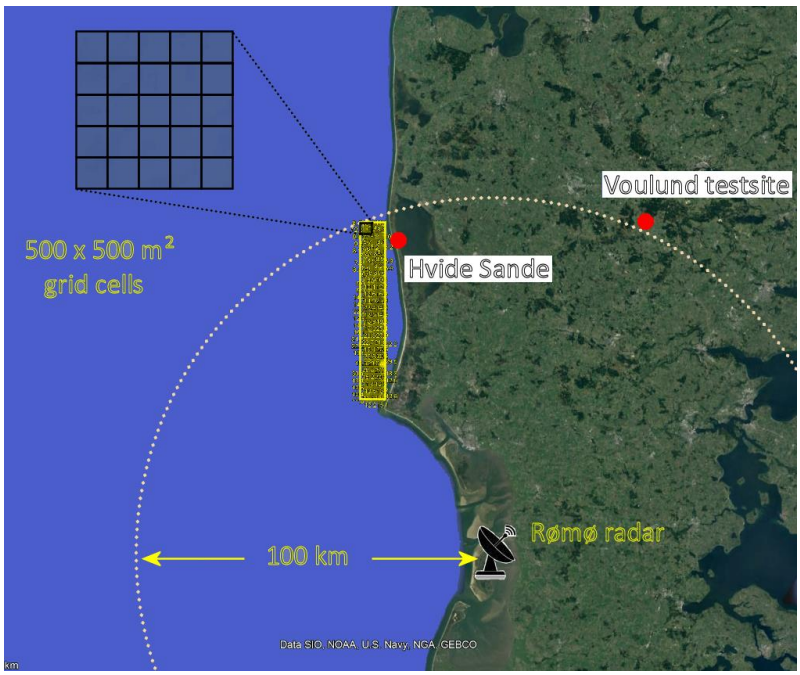

Figure 17: Calculation of rain rate statistics using data from DMI's radar at Rømø for the period June-August 2017. The marked sector consists of a large number of pixels each with an area of 500×500 m^2

Estimation of reliable radar QPE fields requires a relatively large number of adjusting raingauge, and the raingauges have to be not too far away from the area of interest. Especially, adjustment of radar data over sea areas may suffer from the effect of extrapolation due to the lack of raingauge observations in these areas. Therefore, to have control over the uncertainty of the statistics, an offshore sector has been selected which is as close to the coast line and adjusting raingauges as possible.

The sector shown in Figure 17 is composed of a number of grid cells, each consisting of 25×25 pixels. This data structure has been chosen to enable analyses of the spatial variation of rain rates within areas much smaller than the whole sector.

Figure 18 shows the percent of time exceeding a certain rain rate. High uniformity is observed at low rain intensities, which are typically related to stratiform and evenly distributed precipitation. The spatial differences are obviously larger at higher rain rates, probably due to convective rainfall which is usually characterized by major spatial variations. The frequency of high rain rates is very low compared to stratiform precipitation. On the other hand, even relatively short-term impact from heavy rain and hail may have the potential of causing significant damage to wind turbine blades.

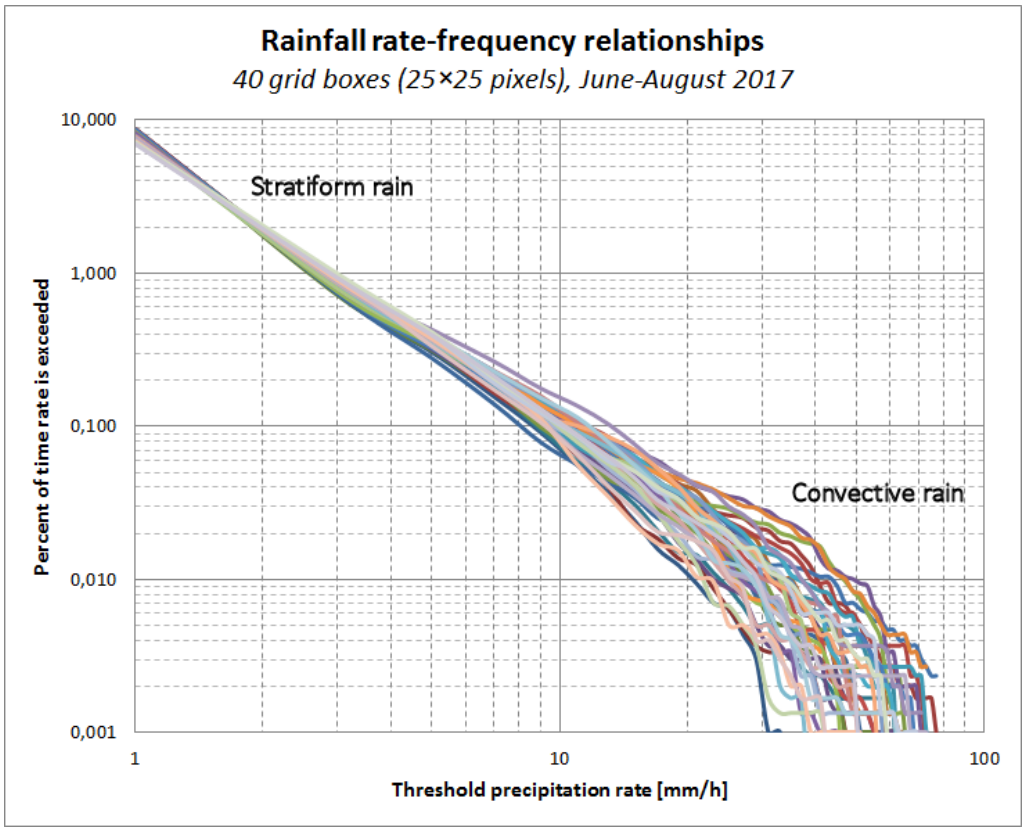

Figure 18: Percent of time rain rate is exceeded calculated on the basis of Rømø radar data for the period June-August 2017. Each graph represents the average rain rate of 25×25 pixels for a number of grid cells within the area shown in Figure 17

During June-August 2017, rain rates larger than 100 mm/h seems to be quite rare in very few cases. This is exemplified in Figure 19 that shows the number of radar pixels with values within certain rain rate intervals. The figure indicates that most of the grid boxes had rain rates up to near 100 mm/h, but the highest rain rates, especially those above 150 mm/h, is only observed in very few cases.

Rain rates above 100 mm/h are most probably caused by so-called sea clutter that is false echoes often seen during stable weather conditions, where the radar beam is bended downwards due to temperature and/or humidity inversions causing reflections from ground targets. Even though the success rate of automatic filtering procedures for false echo removal are normally very high, it is not realistic to achieve a 100 % rate. Because false echoes may be persistent in radar images and that radar data from stable weather periods have been included in the data analyses, the highest values in Figure 19 are most probably not caused by true precipitation. Of this reason, time exceeding the highest rain rates is not included in Figure 18.

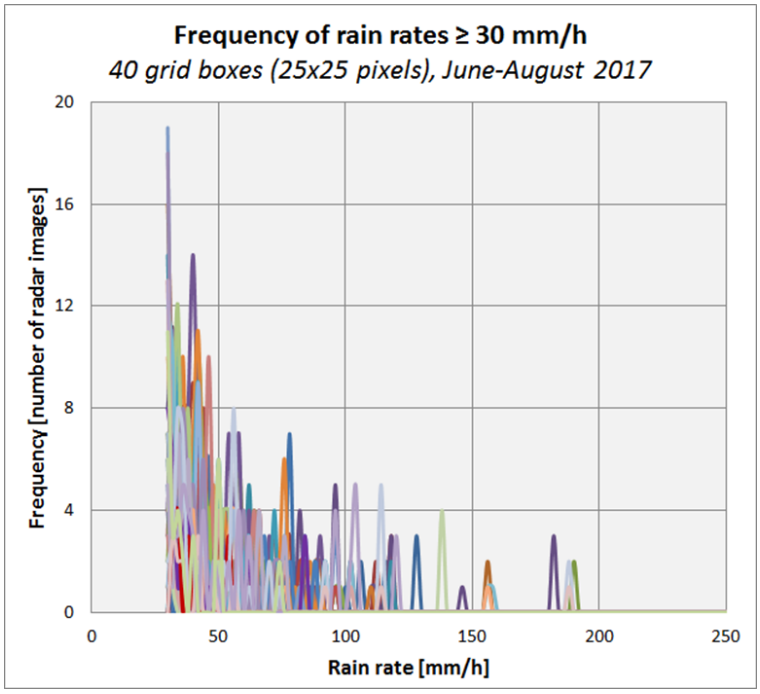

Figure 19: Frequency of rain rates given as number of radar images (Rømø radar data), each representing a period of 10 minutes, for the period June-August 2017. Each graph represents the average frequency 25×25 pixels for a number of grid cells within the area shown in Figure 17

4. Further work and relation to other WP's

4.1 Planned disdrometer campaigns and analyses

A next step of analyzing disdrometer data is the comparison of the precipitation climate of disdrometers installed at different locations. This includes also the calculation of the kinetic energy provided by the precipitation events. Another step is to improve the quality assurance of disdrometer data using weather radar data of DMI. Based on the reflectivity and the hydrometeor classification data of the radar, wrongly classified particles (e.g. insects) can be detected and removed from the disdrometer data. In addition, the comparison of disdrometer data and radar parameters is used to increase the knowledge about the use of radar data for the estimation of the kinetic energy of precipitation events and related erosion classes.

4.2 Analyses of DMI weather station data near wind farms

The plan is to establish precipitation statistics for quite long time series near selected wind farms. Analyses of high resolution data (10-minute observations) over a period of approximately 16 years may be possible for a number of weather stations. The idea is to further examine long term frequencies of erosion critical precipitation near relevant wind farms. PDF's for various precipitation types and rain rates will be calculated at each location for categories of wind speeds. It may be possible to study environmental differences between wind farm sites, and data may be useful as input to wind farm cost-benefit analyses. It may be relevant to

study rain rates in finer time scale than 10 minutes, thus weather radar data will be included in other analyses.

4.3 Further work on weather radar precipitation statistics

An important goal is to establish data series for development of a radar based model for calculation of kinetic energy and erosion classes, and to incorporate new such algorithms in a model for the prediction of potentially damaging weather conditions. This part is closely connected to the disdrometer analyses outlined in section 4.1.

It is expected that the methods for calculating radar-based rain rate statistics will be further developed and improved to achieve as reliable results as possible. In this context, there is still work to do in order to further improve the model for estimation of raingauge adjusted radar rain rates.

In addition, it is expected that radar-based hydrometeor classification will be included in the analyses, among other things to make it possible to calculate probability density functions and statistics on impact time of different intensities from rain, snow, hail and other frozen types of hydrometeors. The analyses and statistical records will be extended to longer periods than the experiments referred to in this report, and to areas near selected wind farms.

4.4 Perspectives for nowcasting of potentially eroding weather conditions

The data series established from disdrometers, weather stations and weather radars will be used to develop a model for conversion of radar parameters to kinetic energy, i.e. erosion classes. Results from WP1 will be included in WP3 for development of a model based on radar data for forecasting of potentially eroding weather conditions.

Required and potentially useful parameters from radar data are rain rate, information about hydrometeor type based on DMI's classification scheme, and Doppler wind speed. In combination with these data, useful information from NWP models will be offshore estimates of wind speed and air temperature, near ground surface as well as higher up in the atmosphere, to support quality assurance and increase understanding of processes.

Due to the lack of agreement between elevated dual-pol radar measurements at larger ranges and the conditions near the ground surface, uncertainties of estimated parameters must be considered and addressed. The challenge is to establish reliable estimates of radar rain rates, Doppler wind speeds and hydrometeor classification at the same height as wind farms.

References

Assouline, S.: Dop size distributions and kinetic energy rates in variable intensity rainfall. *Water Res. Research, Vol. 45, W11501, doi:10.1029/2009WR007927, 2009.*

Atlas, D., Srivastava, R. C., & Sekhon, R. S. (1973). Doppler radar characteristics of precipitation at vertical incidence. *Reviews of Geophysics*, 11(1), 1–35. https://doi.org/10.1029/RG011i001p00001

Badger, M., Peña. A., Hahmann, A.N., Mouche, A., Hasager, C.B. (2016) Extrapolating satellite winds to turbine operating heights. *Journal of Applied Meteorology and Climatology*, doi:10.1175/JAMC-D-15-0197.1

Best, A. C.: The size of distribution of raindrops, *Quart. J. R. Met. Soc., 76, p. 16, 1950.*

Brandes, E. A.: Optimizing rainfall estimates with the aid of radar. *J. Appl. Meteorol., 14, 1339–1345, 1975.*
Chen, B., Wang, J., & Gong, D. (2016). Raindrop size distribution in a midlatitude continental squall line measured by thies optical disdrometers over east China. *Journal of Applied Meteorology and Climatology*, 55(3), 621–634. https://doi.org/10.1175/JAMC-D-15-0127.1

Chumchean, S., Sharma, A., Seed, A.: An integrated approach to error correcion for real-time radar-rainfall estimation. *J. Atmos. Ocean. Technol. 23:67–79, 2006.*

Friedrich, K., Higgins, S., Masters, F. J., & Lopez, C. R. (2013). Articulating and stationary PARSIVEL disdrometer measurements in conditions with strong winds and heavy rainfall. *Journal of Atmospheric and Oceanic Technology*, 30(9), 2063–2080. https://doi.org/10.1175/JTECH-D-12-00254.1

Gill, R., Sørensen, M. B., Bøvith, T.: Hydrometeor Classification using Polarimetric C-band Doppler Weather Radars. *DMI Scientific Report 12-04, 29 p., 2012.*

Haberlandt, U. Geostatistical interpolation of hourly precipitation from rain gauges and radar for a large-scale extreme rainfall event. *J. Hydrol. 332:144–157, 2007.*

He, X., Vejen, F., Stisen, S., Sonnenborg, T., Jensen K.H.: An Operational Weather Radar–Based Quantitative Precipitation Estimation and its Application in Catchment Water Resources Modeling. *Vadose Zone Journal. 10:8-24, doi:10.2136/vzj2010.0034, 2011.*

Hasager, C., Vejen, F.: EROSION, D1.1 Disdrometer in EROSION. *Deliverable D1.1 (Public), Innovationsfonden, Sagsnr. 6154-00018B, 2017.*

Gabella, M., Amitai, E.: Radar rainfall estimates in an alpine environment using different gage-adjustment techniques. *Phys. Chem. Earth B. 25:927–931, 2000.*

Knight, N. C., Heymsfield, A. J., Knight, N. C., & Heymsfield, A. J. (1983). Measurement and Interpretation of Hailstone Density and Terminal Velocity. *Journal of the Atmospheric Sciences.*

Krajewski, W.F. 1987. Cokriging radar-rainfall and rain-gauge data. J. Geophys.
Res. 92:9571–9580.

Kubilay, A., Derome, D., Blocken, B., Carmeliet, J.: CFD simulation and validation of wind-driven rain on a building facade with an Eulerian multiphase model. *Build. Environ., vol. 61, pp. 69–81, http://dx.doi.org/10.1016/j.buildenv.2012.12.005, 2013.*

Lanza, L. G., & Vuerich E. (2009): The WMO field intercomparison of rain intensity gauges. *Atmos. Res.*, 94, 534–543, doi:10.1016/j.atmosres.2009.06.012

Lanzinger, E., Theel, M., and Windolph H. (2006): Rainfall amount and intensity measured by the Thies laser precipitation monitor. *TECO-2006: WMO Tech. Conf. on Meteorological and Environmental Instruments and Methods of Observation*, Geneva, Switzerland, WMO, 3(3), WMO IOM-94, 9 pp., https://www.wmo.int/pages/prog/www/IMOP/ publications/IOM-94-TECO2006/3(3)_Lanzinger_Germany.pdf.

Locatelli, J. D., & Hobbs, P. V. (1974). Fall speeds and masses of solid precipitation particles. *J. Geophys. Res.*, 79(15), 2185–2197. https://doi.org/10.1029/JC079i015p02185

Michelson, D. B., T. Andersson, J. Koistinen, C. G. Collier, J. Riedl, J. Szturc, U. Gjertsen, A. Nielsen, S. Overgaard: BALTEX Radar Data Centre Products and their Methodologies. *SMHI Reports Meteorology and Climatology, No. 90, 75p, 2000.*

Rosenfeld, D., Wolff, D. B. , Amitai, E.: The window probability matching method for rainfall measurements with radar. *J. Appl. Meteorol. 33:682–693, 1994*.

Šálek, M., Cheze, J.-L., Handwerker, J., Delobbe, L., Uijlenhoet, R.: Radar techniques for identifying precipitation type and estimating quantity of precipitation. *Document of COST Action 717, WG 1, Task WG 1-2, 51p, 2004.*

Sinclair, S., Pegram G.: Combining radar and rain gauge rainfall estimates using conditional merging. *Atmos. Sci. Lett. 6:19–22, 2005*.

Smith, J.A., Krajewski, W. F.: Estimation of the mean field bias of radar rainfall estimates. *J. Appl. Meteorol. 30:397–412, 1991*.

Straka, J. M., Zrnic, D. S., Ryzhkov, A. V.: Bulk Hydrometeor Classification and Quantification Using Polarimetric Radar Data: Synthesis of Relations. *J. Appl. Met., Vol. 39, 1341-1372, 2000.*

Testik, F. Y., & Pei, B. (2017). Wind Effects on the Shape of Raindrop Size Distribution. *Journal of Hydrometeorology*, 18(5). https://doi.org/10.1175/JHM-D-16-0211.1

Vaisala: Weather Sensor FD12P, User's Guide. *M210296en-A, Vaisala, 154p, 2002*.